

## **Evolution of Anisotropic Displacement Parameters and Superconductivity with Chemical Pressure in BiS<sub>2</sub>-Based REO<sub>0.5</sub>F<sub>0.5</sub>BiS<sub>2</sub> (RE = La, Ce, Pr, and Nd)**

Yoshikazu Mizuguchi<sup>1</sup>, Kazuhisa Hoshi<sup>1</sup>, Yosuke Goto<sup>1</sup>, Akira Miura<sup>2</sup>, Kiyoharu Tadanaga<sup>2</sup>, Chikako Moriyoshi<sup>3</sup>, Yoshihiro Kuroiwa<sup>3</sup>

1. Graduate School of Science and Engineering, Tokyo Metropolitan University, 1-1, Minami-osawa, Hachioji 192-0397, Japan.
2. Faculty of Engineering, Hokkaido University, Kita-13, Nishi-8, Kita-ku, Sapporo, Hokkaido 060-8628, Japan.
3. Department of Physical Science, Hiroshima University, 1-3-1 Kagamiyama, Higashihiroshima, Hiroshima 739-8526, Japan.

\* Corresponding author: Yoshikazu Mizuguchi (mizugu@tmu.ac.jp)

### **Abstract**

In order to understand the mechanisms behind the emergence of superconductivity by the chemical pressure effect in REO<sub>0.5</sub>F<sub>0.5</sub>BiS<sub>2</sub> (RE = La, Ce, Pr, and Nd), where bulk superconductivity is induced by the substitutions with a smaller-radius RE, we performed synchrotron powder X-ray diffraction, and analyzed the crystal structure and anisotropic displacement parameters. With the decrease of the RE<sup>3+</sup> ionic radius, the in-plane disorder of the S1 sites significantly decreased, very similar to the trend observed in the Se-substituted systems: LaO<sub>0.5</sub>F<sub>0.5</sub>BiS<sub>2-x</sub>Se<sub>x</sub> and Eu<sub>0.5</sub>La<sub>0.5</sub>FBiS<sub>2-x</sub>Se<sub>x</sub>. Therefore, the emergence of bulk superconductivity upon the suppression of the in-plane disorder at the chalcogen sites is a universal scenario for the BiCh<sub>2</sub>-based superconductors. In addition, we indicated that the amplitude of vibration along the *c*-axis of the in-plane chalcogen sites may be related to the *T<sub>c</sub>* in the BiCh<sub>2</sub>-based superconductors.

BiS<sub>2</sub>-based layered compounds have been extensively studied owing to the discovery of superconductivity in electron-doped phases and their relatively high transition temperatures ( $T_c$ ), as high as 11 K [1–3]. A typical parent phase of the BiS<sub>2</sub>-based superconductor is REOBiS<sub>2</sub> (RE: rare earth element), which has a layered structure composed of alternate stacks of REO insulating (blocking) layers and BiS<sub>2</sub> electrically conducting layers; it has a band gap of ~1 eV [2–5]. Electron carriers can be introduced in the BiS<sub>2</sub> layers by partial substitutions of the elements of the blocking REO layers [6–11]. For example, in LaO<sub>1-x</sub>F<sub>x</sub>BiS<sub>2</sub>, the partial substitutions of O<sup>2-</sup> sites with F<sup>-</sup> generate electron carriers; the carrier concentration can be manipulated by varying the amount of substituted F [2]. Bulk superconductivity with a large shielding fraction in the magnetization measurements was not observed in electron-doped LaO<sub>1-x</sub>F<sub>x</sub>BiS<sub>2</sub> samples prepared using the solid-state reaction method at ambient pressure; however, filamentary superconducting states with a small shielding volume fraction were observed at  $T_c$  ~2.5 K [2]. In addition, the observed temperature dependence of the electrical resistivity was not metallic-like; it showed a weakly localized behavior in LaO<sub>1-x</sub>F<sub>x</sub>BiS<sub>2</sub>, although band calculations suggested that the electron-doped LaO<sub>1-x</sub>F<sub>x</sub>BiS<sub>2</sub> should be metal [4, 5, 12]. These results suggested that the doped electrons were localized by the effect of structural disorder.

In order to induce bulk superconductivity in LaO<sub>1-x</sub>F<sub>x</sub>BiS<sub>2</sub>, high pressure effects can be employed. The application of an external pressure induces bulk superconductivity with a  $T_c$  of ~10 K [13–15]. In addition, samples annealed under a high pressure (~2 GPa) also exhibit bulk superconductivity with a  $T_c$  of ~10 K [2, 16–18]. The emergence of bulk superconductivity and increase of  $T_c$  in the high-pressure phase can be attributed to the structural phase transition from the tetragonal low- $T_c$  phase to the monoclinic high- $T_c$  phase [13].

Another approach to induce bulk superconductivity in the LaO<sub>1-x</sub>F<sub>x</sub>BiS<sub>2</sub> system is to introduce a chemical pressure by an isovalent substitution, such as Ch (Ch: S, Se) and/or RE site substitutions. In LaO<sub>0.5</sub>F<sub>0.5</sub>BiS<sub>2-x</sub>Se<sub>x</sub>, the substitutions of Se for the S sites induces bulk superconductivity with a  $T_c$  of ~3.8 K [19, 20]. Another isovalent substitution is the RE site substitution. With the decrease of the RE<sup>3+</sup> (mean) ionic radius in REO<sub>0.5</sub>F<sub>0.5</sub>BiS<sub>2</sub>, the BiS<sub>2</sub> layer becomes compressed, in particular along the *ab*-plane direction, and bulk superconductivity is induced [21]. As the isovalent substitution does not significantly affect the carrier concentration, the structural optimization induces superconductivity in the Ch- and RE-substituted systems. In order to analyze the essential factor for the emergence of the superconductivity, we considered the commonality of the chemical pressure effects between the Ch- and RE substitutions, by introducing the concept of an in-plane chemical pressure [22].

The emergence of the bulk superconductivity in the LaO<sub>0.5</sub>F<sub>0.5</sub>BiS<sub>2-x</sub>Se<sub>x</sub> system was explained by the decrease in the in-plane disorder of the chalcogen sites with the increase of the Se content, which was detected through a crystal structure analysis of the synchrotron X-ray diffraction (SXRD) pattern [23] and extended X-ray absorption fine structure (EXAFS) [24]. A similar relationship between the in-plane disorder and emergence of superconductivity was observed in Eu<sub>0.5</sub>La<sub>0.5</sub>FBiS<sub>2-x</sub>Se<sub>x</sub> [25–27].

For both systems, the Se substitutions induced a metallic electrical conductivity. Therefore, the in-plane disorder of the in-plane chalcogen sites is the factor that prevented the emergence of superconductivity and metallic conductivity in  $\text{LaO}_{1-x}\text{F}_x\text{BiS}_2$ . Therefore, we expect that a similar suppression of the in-plane disorder at the in-plane S sites (S1 site in Fig. 1(b)) can be attributed with the emergence of superconductivity in the RE-substituted systems. Neutron diffraction and pair distribution function analysis revealed the presence of the in-plane disorder and its relationship with the superconductivity, where RE is La or Nd [28, 29]. In addition, EXAFS measurements reveled a suppression of the Bi-S1-bond-disorder with the decrease of the  $\text{RE}^{3+}$  radius [30]. Therefore, in this study, we investigated the atomic displacement parameters of  $\text{REO}_{0.5}\text{F}_{0.5}\text{BiS}_2$  with  $\text{RE} = \text{La}, \text{Ce}, \text{Pr}$ , and Nd using SXRD and Rietveld refinement. Anisotropic analyses of the displacement parameters revealed that the in-plane displacement of S1 was very large for  $\text{RE} = \text{La}$  and gradually decreased with the decrease of the  $\text{RE}^{3+}$  ionic radius. This behavior is equal to that of the Se substitution. Therefore, the suppression of the in-plane disorder at the in-plane S1 (or Ch1) sites and emergence of superconductivity by the chemical pressure effects are universal for  $\text{BiCh}_2$ -based superconductors. As unconventional superconductivity states are likely to appear in both Ch-substituted  $\text{La(O,F)}\text{Bi(S,Se)}_2$  and RE-substituted  $\text{REO}_{0.5}\text{F}_{0.5}\text{BiS}_2$  systems [31–33], the universality revealed in this study could be employed to further understand the mechanisms of the superconductivity in the  $\text{BiCh}_2$ -based superconductors.

Polycrystalline samples of  $\text{REO}_{0.5}\text{F}_{0.5}\text{BiS}_2$  with  $\text{RE} = \text{La}, \text{Ce}, \text{Pr}$ , and Nd were prepared using the solid-state-reaction method [2, 6–9]. A mixture of the starting materials was pressed into a pellet and annealed at 700 °C for 20 h in an evacuated quartz tube. SXRD was performed at the beamline BL02B2, SPring-8 at a wavelength of 0.49559 Å (proposal No.: 2017B1211). The SXRD experiments were performed with a sample rotator system at room temperature; the diffraction data were collected using a high-resolution one-dimensional semiconductor detector (multiple MYTHEN system [34]) with a step size of  $2\theta = 0.006^\circ$ . The crystal structure parameters were refined using the Rietveld method with the RIETAN-FP program [35]. Images with schematic models of the crystal structures were produced using VESTA [36].

Figure 1(a) shows the superconductivity phase diagram of  $\text{REO}_{0.5}\text{F}_{0.5}\text{BiS}_2$  as a function of the  $\text{RE}^{3+}$  ionic radius. The filamentary superconducting states observed for La are suppressed for Ce. A polycrystalline sample of  $\text{CeO}_{0.5}\text{F}_{0.5}\text{BiS}_2$  with 50% F substitution does not show superconductivity; however,  $\text{CeO}_{0.3}\text{F}_{0.7}\text{BiS}_2$  with 70% F substitution shows bulk superconductivity upon the effect of high pressure [37]. As reported in Ref. 21, bulk superconductivity of  $\text{REO}_{0.5}\text{F}_{0.5}\text{BiS}_2$  appears at an  $\text{RE}^{3+}$ -radius of ~113 pm, which corresponds to  $\text{RE} = \text{Pr}$  or  $\text{Ce}_{0.5}\text{Nd}_{0.5}$ .  $T_c$  increases with the decrease of the  $\text{RE}^{3+}$  radius. The temperature dependences of the magnetization for the samples used in this study are

shown in Figure S1 of the Supplemental Material [38].  $T_c$  values estimated from the magnetization measurements are represented with the larger circles in Fig. 1(a), which are in agreement with the results of a previous study [21].

Figure 2 shows the SXRD patterns and Rietveld refinement results for RE = (a) La, (b) Ce, (c) Pr, and (d) Nd. The Rietveld refinements were performed using a tetragonal  $P4/nmm$  model. For RE = La, Ce, and Pr, a small portion (smaller than 4%) of  $\text{REF}_3$  impurity phases was detected, and a two-phase analysis was performed. For RE = Nd, unidentified impurity peaks were observed; hence, we analyzed the data for RE = Nd by a single-phase analysis. For all data, excellent fitting was also obtained at higher angles, required for a precise refinement of the displacement parameters.

Figures 3(a) and 3(b) show the dependences of the lattice constants  $a$  and  $c$  as a function of the  $\text{RE}^{3+}$  ionic radius. The lattice constant  $a$  linearly decreases with the decrease of the  $\text{RE}^{3+}$  radius. However, the lattice constant  $c$  does not exhibit a clear correlation with the  $\text{RE}^{3+}$  radius. Figure 3(c) shows the dependences of the Bi-S1 and Bi-S2 bond distances as a function of the  $\text{RE}^{3+}$  ionic radius (See Fig. 1(b) for the labeling of the S sites). It can be noticed that the in-plane Bi-S1 distance decreases with the decrease of the  $\text{RE}^{3+}$  radius, owing to the linear decrease in the lattice constant  $a$ . In contrast, Bi-S2 and interplane Bi-S1 distances do not decrease upon the introduction of chemical pressure, which may be related with the nonlinear change in the lattice constant  $c$ . However, as reported in Ref. 22, the essential factor for the emergence of superconductivity in the  $\text{REO}_{0.5}\text{F}_{0.5}\text{BiCh}_2$  systems is the in-plane chemical pressure. In the considered  $\text{REO}_{0.5}\text{F}_{0.5}\text{BiS}_2$  system, the amplitude of the in-plane chemical pressure is directly determined by the in-plane Bi-S1 distance. Therefore, we can analyze the relationship between the chemical pressure, superconductivity, and in-plane disorder using the considered samples.

We performed Rietveld refinements with anisotropic displacement parameters  $U_{11}$  and  $U_{33}$  for the in-plane Bi and S1 sites. Figure 4(c) illustrates  $U_{11}$  and  $U_{33}$  using a schematic model with RE = Pr. For the other sites, isotropic displacement parameters were assumed for the refinements. The obtained  $U_{11}$  and  $U_{33}$  for the Bi and S1 sites are plotted in Figs. 4(a) and 4(b), respectively. As expected,  $U_{11}$  for the S1 sites is very large for RE = La, and decreases with the decrease of the  $\text{RE}^{3+}$  radius, a very similar trend with that observed for  $U_{11}$  for the in-plane chalcogen sites in  $\text{LaO}_{0.5}\text{F}_{0.5}\text{BiS}_{2-x}\text{Se}_x$  [23]. Therefore, the large suppression of the in-plane disorder at the in-plane chalcogen sites can be universally attributed with the emergence of bulk superconductivity in the  $\text{REO}_{0.5}\text{F}_{0.5}\text{BiCh}_2$  systems. It is worth noting that  $U_{11}$  for the Bi sites slightly increases with the decrease of the  $\text{RE}^{3+}$  radius. Recently, Athauda et al. proposed that the increase in the in-plane displacement of Bi may be attributed with the superconductivity in  $\text{NdO}_{1-x}\text{F}_x\text{BiS}_2$ , while the in-plane displacement of S1 would induce carrier localization [29]. Our analysis also suggests that the increase of the in-plane displacement of the Bi sites may be related with the enhanced  $T_c$  for RE = Pr and Nd. Similar trend is observed for  $U_{33}$  in Fig. 4(b). Although  $U_{33}$  for the Bi sites does not considerably change with the decrease of the  $\text{RE}^{3+}$  radius,

$U_{33}$  for the S1 sites dramatically changes with the replacement of the RE. It is worth noting that the evolution of  $U_{33}$  for the S1 sites seems to be linked with the enhancement of  $T_c$ . A similar evolution of the displacement ellipsoids is observed in Se-substituted  $\text{LaO}_{0.5}\text{F}_{0.5}\text{BiSSe}$ , as shown in Fig. 5. Both RE and Ch substitutions suppress  $U_{11}$  for the Ch1 sites; however, they enhance  $U_{33}$  for the Ch1 sites. This trend may suggest that the amplitude of the one-dimensional large vibration of S1 is correlated with the  $T_c$  in this system. If this is valid, then the  $T_c$  increases when the phonon frequency decreases with the increase of the amplitude of the S1 vibration along the  $c$ -axis. This scenario is not consistent with the conventional phonon-mediated mechanisms. It is consistent with the isotope effect; no isotope effect was observed for the  $\text{LaO}_{0.6}\text{F}_{0.4}\text{Bi}(\text{S},\text{Se})_2$  samples with  $^{76}\text{Se}$  and  $^{80}\text{Se}$  isotopes [31]. If such large vibrations of Ch1 are related with the enhancement of  $T_c$ , charge fluctuation should occur in the superconducting Bi-Ch1 plane. Then, the pairing phenomena mediated by charge fluctuations, proposed by theoretical and experimental studies [28, 29, 32, 39], may occur in the  $\text{BiCh}_2$ -based system.

In conclusion, we investigated the crystal structure and anisotropic displacement parameters of  $\text{REO}_{0.5}\text{F}_{0.5}\text{BiS}_2$  with  $\text{RE} = \text{La, Ce, Pr, and Nd}$ , where bulk superconductivity is induced by substitutions with a smaller-radius RE, such as Pr or Nd. With the decrease of the  $\text{RE}^{3+}$  ionic radius, the lattice constant  $a$  and in-plane Bi-S1 distance monotonically decreased, which generated the in-plane chemical pressure effect. With the decrease of the  $\text{RE}^{3+}$  radius, the in-plane disorder of the S1 sites significantly decreased. This trend is very similar to those observed for Se-substituted  $\text{LaO}_{0.5}\text{F}_{0.5}\text{BiS}_{2-x}\text{Se}_x$  and  $\text{Eu}_{0.5}\text{La}_{0.5}\text{FBiS}_{2-x}\text{Se}_x$ . Therefore, the emergence of bulk superconductivity upon the suppression of the in-plane disorder at the Ch1 sites seems to be a universal scenario for the  $\text{BiCh}_2$ -based superconductors. The analyses of the displacement parameters along the  $c$ -axis indicated that the amplitude of the one-dimensional vibration of S1 (or Ch1) along the  $c$ -axis was correlated with  $T_c$  in the  $\text{BiCh}_2$ -based superconductors.

#### Acknowledgements

We would like to thank O. Miura for his experimental support. This study was partially supported by the Grants-in-Aid for Scientific Research (Nos. 15H05886, 16H04493, 16K17944, 17K19058, and 17H04950) and JST-CREST (No. JPMJCR16Q6), Japan.

## References

- 1) Y. Mizuguchi, H. Fujihisa, Y. Gotoh, K. Suzuki, H. Usui, K. Kuroki, S. Demura, Y. Takano, H. Izawa, and O. Miura, Phys. Rev. B **86**, 220510 (2012).
- 2) Y. Mizuguchi, S. Demura, K. Deguchi, Y. Takano, H. Fujihisa, Y. Gotoh, H. Izawa, and O. Miura , J. Phys. Soc. Jpn. **81**, 114725 (2012).
- 3) Y. Mizuguchi, J. Phys. Chem. Solids **84**, 34 (2015).
- 4) H. Usui, K. Suzuki, and K. Kuroki, Phys. Rev. B **86**, 220501 (2012).
- 5) H. Usui and K. Kuroki, Nov. Supercond. Mater. **1**, 50 (2015).
- 6) J. Xing, S. Li, X. Ding, H. Yang, and H. H. Wen, Phys. Rev. B **86**, 214518 (2012).
- 7) R. Jha, A. Kumar, S. K. Singh, and V. P. S. Awana, J. Supercond. Nov. Magn. **26**, 499 (2013).
- 8) S. Demura, Y. Mizuguchi, K. Deguchi, H. Okazaki, H. Hara, T. Watanabe, S. J. Denholme, M. Fujioka, T. Ozaki, H. Fujihisa, Y. Gotoh, O. Miura, T. Yamaguchi, H. Takeya, and Y. Takano, J. Phys. Soc. Jpn. **82**, 033708 (2013).
- 9) D. Yazici, K. Huang, B. D. White, A. H. Chang, A. J. Friedman, and M. B. Maple, Philos. Mag. **93**, 673 (2012).
- 10) D. Yazici, K. Huang, B. D. White, I. Jeon, V. W. Burnett, A. J. Friedman, I. K. Lum, M. Nallaiyan, S. Spagna, and M. B. Maple, Phys. Rev. B **87**, 174512 (2013).
- 11) R. Sogabe, Y. Goto, A. Nishida, T. Katase, and Y. Mizuguchi, arXiv:1709.00892.
- 12) B. Li, Z. W. Xing, and G. Q. Huang, EPL **101**, 47002 (2013).
- 13) T. Tomita, M. Ebata, H. Soeda, H. Takahashi, H. Fujihisa, Y. Gotoh, Y. Mizuguchi, H. Izawa, O. Miura, S. Demura, K. Deguchi, and Y. Takano, J. Phys. Soc. Jpn. **83**, 063704 (2014).
- 14) Y. Fang, D. Yazici, B. D. White, and M. B. Maple, Phys. Rev. B **92**, 094507 (2015).
- 15) R. Jha, H. Kishan, and V. P. S. Awana, J. Phys. Chem. Solids **84**, 17 (2015).
- 16) K. Deguchi, Y. Mizuguchi, S. Demura, H. Hara, T. Watanabe, S. J. Denholme, M. Fujioka, H. Okazaki, T. Ozaki, H. Takeya, T. Yamaguchi, O. Miura, and Y. Takano, EPL **101**, 17004 (2013).
- 17) Y. Mizuguchi, T. Hiroi, J. Kajitani, H. Takatsu, H. Kadowaki, and O. Miura, J. Phys. Soc. Jpn. **83**, 053704 (2014).
- 18) J. Kajitani, K. Deguchi, A. Omachi, T. Hiroi, Y. Takano, H. Takatsu, H. Kadowaki, O. Miura, Y. Mizuguchi, Solid State Commun. **181**, 1 (2014)
- 19) X. C. Wang, D. Y. Chen, Q. Guo, J. Yu, B. B. Ruan, Q. G. Mu, G. F. Chen, and Z. A. Ren, arXiv:1404.7562.
- 20) T. Hiroi, J. Kajitani, A. Omachi, O. Miura, and Y. Mizuguchi, J. Phys. Soc. Jpn **84**, 024723 (2015).
- 21) J. Kajitani, T. Hiroi, A. Omachi, O. Miura, and Y. Mizuguchi, J. Phys. Soc. Jpn. **84**, 044712 (2015).
- 22) Y. Mizuguchi, A. Miura, J. Kajitani, T. Hiroi, O. Miura, K. Tadanaga, N. Kumada, E. Magome, C. Moriyoshi, and Y. Kuroiwa, Sci. Rep. **5**, 14968 (2015).

- 23) K. Nagasaka, A. Nishida, R. Jha, J. Kajitani, O. Miura, R. Higashinaka, T. D. Matsuda, Y. Aoki, A. Miura, C. Moriyoshi, Y. Kuroiwa, H. Usui, K. Kuroki, and Y. Mizuguchi, *J. Phys. Soc. Jpn.* **86**, 074701 (2017).
- 24) E. Paris, Y. Mizuguchi, M. Hacisalihoglu, T. Hiroi, B. Joseph, G. Aquilanti, O. Miura, T. Mizokawa, N. Saini, *J. Phys.: Condens. Matter* **29**, 145603 (2017).
- 25) G. Jinno, R. Jha, A. Yamada, R. Higashinaka, T. D. Matsuda, Y. Aoki, M. Nagao, O. Miura, and Y. Mizuguchi, *J. Phys. Soc. Jpn.* **85**, 124708 (2016).
- 26) K. Nagasaka, G. Jinno, O. Miura, A. Miura, C. Moriyoshi, Y. Kuroiwa, and Y. Mizuguchi, *J. Phys.: Conf. Ser.* **871**, 012007 (2017).
- 27) Y. Mizuguchi, E. Paris, T. Wakita, G. Jinno, A. Puri, K. Terashima, B. Joseph, O. Miura, T. Yokoya, and N. L. Saini, *Phys. Rev. B* **95**, 064515 (2017).
- 28) A. Athauda, J. Yang, S. Lee, Y. Mizuguchi, K. Deguchi, Y. Takano, O. Miura, and D. Louca, *Phys. Rev. B* **91**, 144112 (2014).
- 29) A. Athauda, Y. Mizuguchi, M. Nagao, J. Neufeind, and D. Louca, arXiv:1708.03957.
- 30) Y. Mizuguchi, E. Paris, T. Sugimoto, A. Iadecola, J. Kajitani, O. Miura, T. Mizokawa, and N. L. Saini, *Phys. Chem. Chem. Phys.* **17**, 22090 (2015).
- 31) K. Hoshi, Y. Goto, and Y. Mizuguchi, arXiv:1708.08252.
- 32) Y. Ota, K. Okazaki, H. Q. Yamamoto, T. Yamamoto, S. Watanabe, C. Chen, M. Nagao, S. Watauchi, I. Tanaka, Y. Takano, and S. Shin, *Phys. Rev. Lett.* **118**, 167002 (2017).
- 33) C. Morice, R. Akashi, T. Koretsune, S. S. Saxena, and R. Arita, *Phys. Rev. B* **95**, 180505 (2017).
- 34) S. Kawaguchi, M. Takemoto, K. Osaka, E. Nishibori, C. Moriyoshi, Y. Kubota, Y. Kuroiwa, and K. Sugimoto, *Rev. Sci. Instr.* **88**, 085111 (2017).
- 35) F. Izumi and K. Momma, *Solid State Phenom.* **130**, 15 (2007).
- 36) K. Momma and F. Izumi, *J. Appl. Crystallogr.* **41**, 653 (2008).
- 37) S. Demura, K. Deguchi, Y. Mizuguchi, K. Sato, R. Honjyo, A. Yamashita, T. Yamaki, H. Hara, T. Watanabe, S. J. Denholme, M. Fujioka, H. Okazaki, T. Ozaki, O. Miura, T. Yamaguchi, H. Takeya, and Y. Takano, *J. Phys. Soc. Jpn.* **84**, 024709 (2015).
- 38) [Supplemental Materials] Figure S1. Temperature dependences of the magnetization for  $\text{REO}_{0.5}\text{F}_{0.5}\text{BiS}_2$  ( $\text{RE} = (\text{a}) \text{La}, (\text{b}) \text{Ce}, (\text{c}) \text{Pr}, \text{and} (\text{d}) \text{Nd}$ ).
- 39) K. Suzuki, H. Usui, K. Kuroki, and H. Ikeda, *Phys. Rev. B* **96**, 024513 (2017).

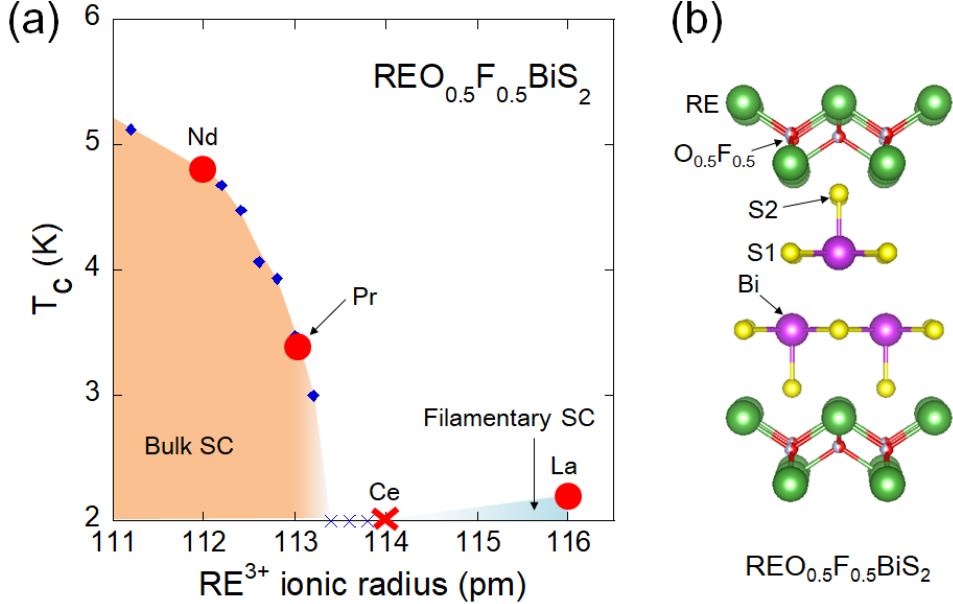


Fig. 1. (Color online) (a) Superconductivity phase diagram of  $\text{REO}_{0.5}\text{F}_{0.5}\text{BiS}_2$  as a function of the  $\text{RE}^{3+}$  ionic radius with a coordination number of 6. Data points for  $\text{Ce}_{1-x}\text{Nd}_x\text{O}_{0.5}\text{F}_{0.5}\text{BiS}_2$  and  $\text{Nd}_{1-x}\text{Sm}_x\text{O}_{0.5}\text{F}_{0.5}\text{BiS}_2$  have been published in Ref. 26. Bulk and filamentary SC denote the bulk and filamentary superconducting states with weak diamagnetic signals, respectively. (b) Schematic model of the crystal structure of  $\text{REO}_{0.5}\text{F}_{0.5}\text{BiS}_2$ .

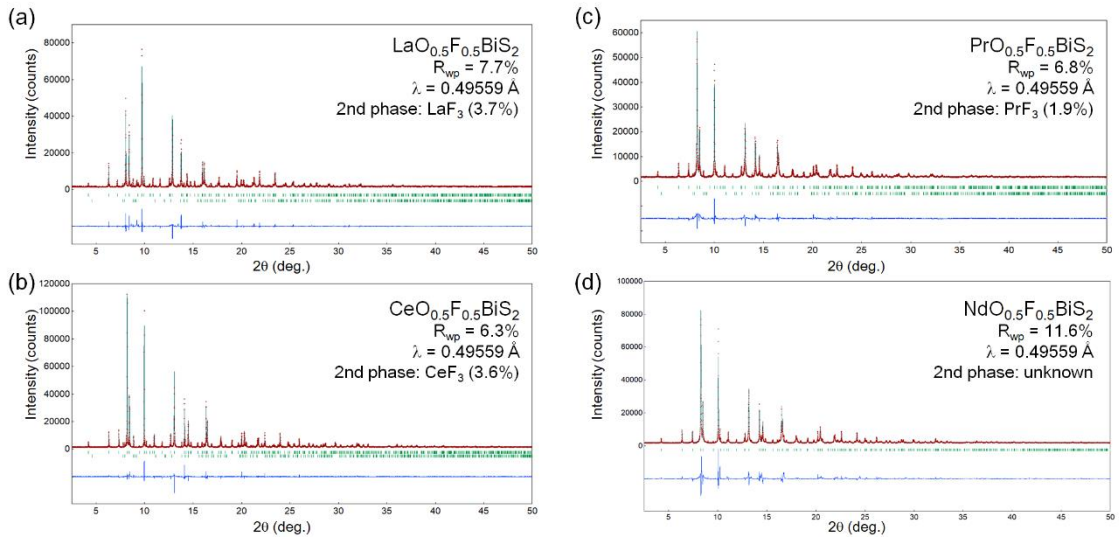


Fig. 2. (Color online) SXRD patterns for (a)  $\text{LaO}_{0.5}\text{F}_{0.5}\text{BiS}_2$ , (b)  $\text{CeO}_{0.5}\text{F}_{0.5}\text{BiS}_2$ , (c)  $\text{PrO}_{0.5}\text{F}_{0.5}\text{BiS}_2$ , and (d)  $\text{NdO}_{0.5}\text{F}_{0.5}\text{BiS}_2$ .

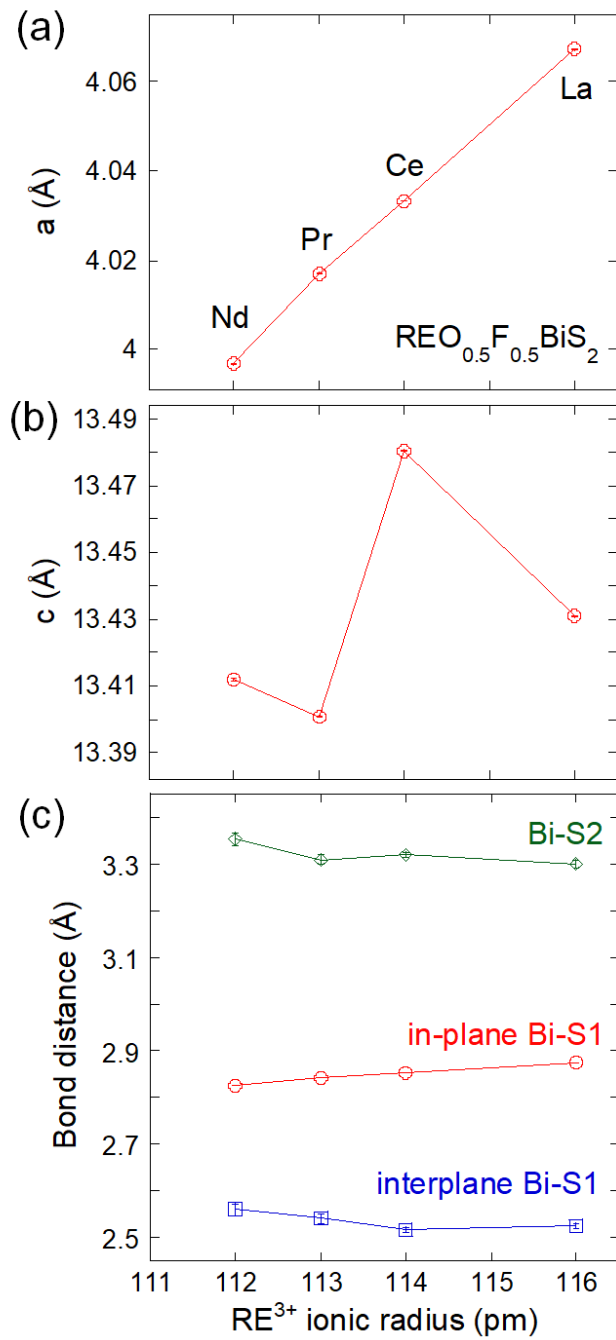


Fig. 3. (Color online) Dependences of the lattice constants (a)  $a$  and (b)  $c$ , and (c) Bi-S bond distances, as a function of the  $\text{RE}^{3+}$  ionic radius.

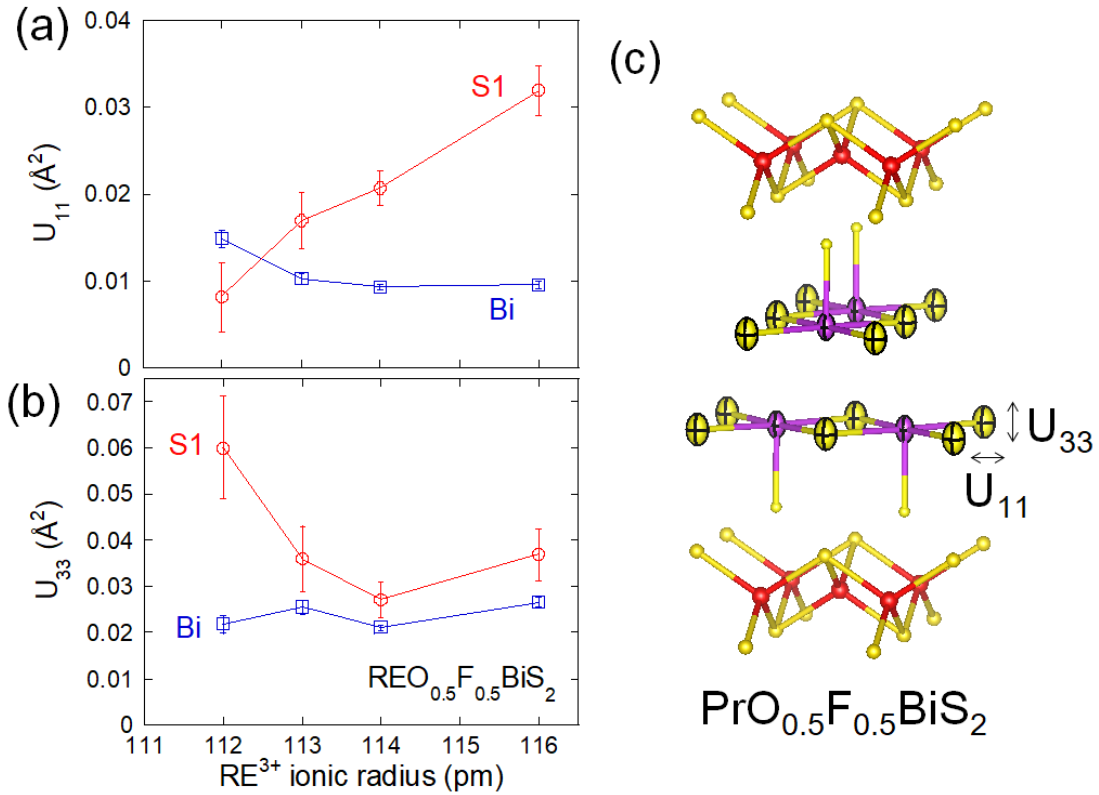


Fig. 4. (Color online) Dependences of the anisotropic displacement parameters (a)  $U_{11}$  and (b)  $U_{33}$  for the Bi and S1 sites as a function of the RE<sup>3+</sup> ionic radius. (c) Schematic model of the crystal structure of  $\text{PrO}_{0.5}\text{F}_{0.5}\text{BiS}_2$ ; 90%-probability displacement ellipsoids are outlined.

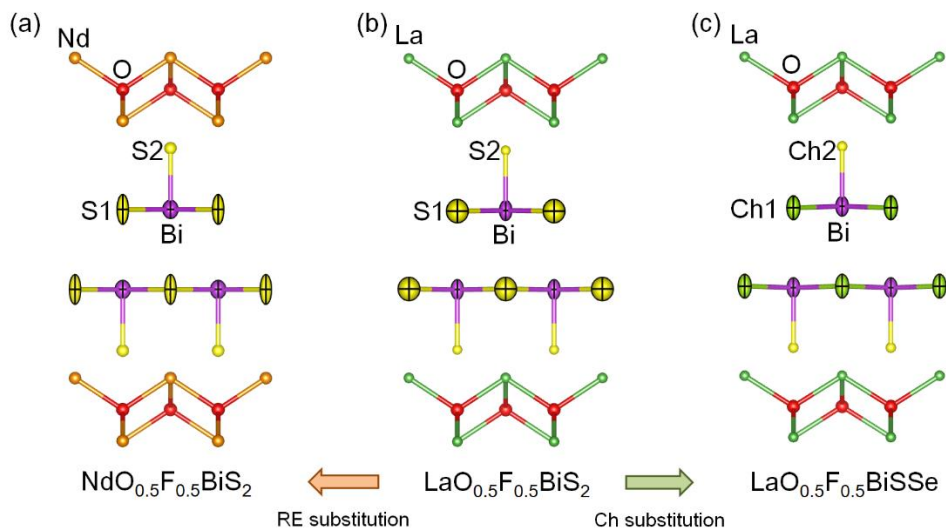


Fig. 5. (Color online) Evolution of the displacement ellipsoids (90% probability) by the effect of chemical pressure (RE or Ch substitutions) in the  $\text{REO}_{0.5}\text{F}_{0.5}\text{BiCh}_2$  system. For  $\text{LaO}_{0.5}\text{F}_{0.5}\text{BiSSe}$ , Se selectively occupies the Ch1 sites.

## Supplemental Materials

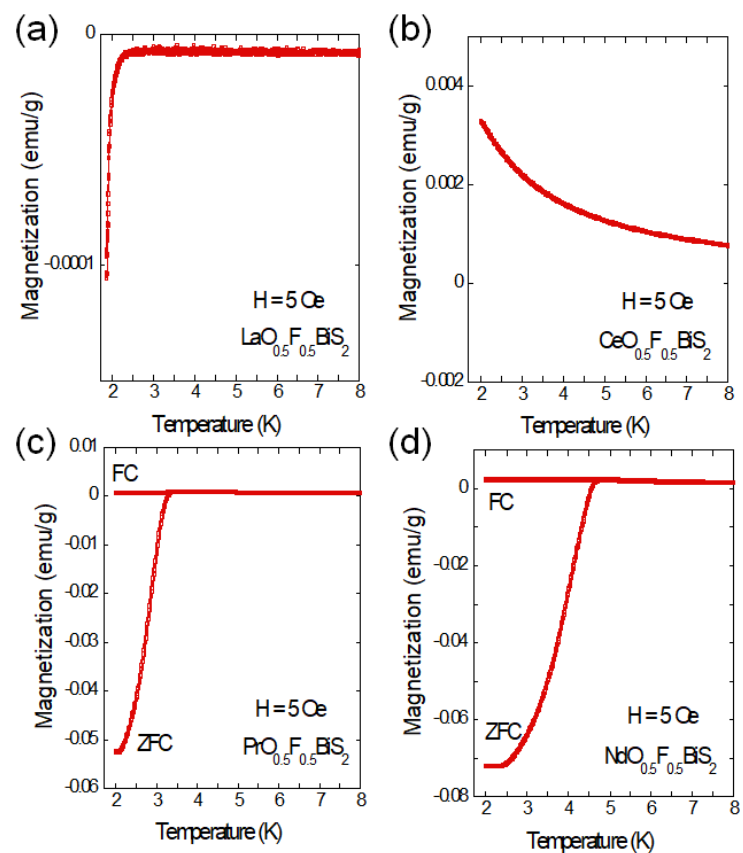


Fig. S1. Temperature dependence of the magnetization for (a)  $\text{LaO}_{0.5}\text{F}_{0.5}\text{BiS}_2$ , (b)  $\text{CeO}_{0.5}\text{F}_{0.5}\text{BiS}_2$ , (c)  $\text{PrO}_{0.5}\text{F}_{0.5}\text{BiS}_2$ , and (d)  $\text{NdO}_{0.5}\text{F}_{0.5}\text{BiS}_2$ .

Table SI. Crystal structure parameters for  $\text{REO}_{0.5}\text{F}_{0.5}\text{BiS}_2$  obtained by the Rietveld refinements. The atomic coordinate for the oxygen (fluorine) site is (0, 0, 0), and the  $U_{\text{iso}}$  is fixed as  $0.013 \text{ \AA}^2$ . The atomic coordinate for other sites is (0, 0.5,  $z$ ).

RE	La	Ce	Pr	Nd
Space group	$P4/nmm$	$P4/nmm$	$P4/nmm$	$P4/nmm$
$a$ ( $\text{\AA}$ )	4.06732(4)	4.03329(2)	4.01708(6)	3.99671(8)
$c$ ( $\text{\AA}$ )	13.4310(2)	13.48059(10)	13.4008(3)	13.4118(4)
$V$ ( $\text{\AA}^3$ )	222.189 (4)	219.294(3)	216.247(6)	214.236(8)
$R_{\text{wp}}$ (%)	7.7	6.3	6.8	11.6
$z$ (RE)	0.09960(10)	0.09656(7)	0.09822(12)	0.0981(2)
$z$ (Bi)	0.62381(9)	0.62519(7)	0.62468(13)	0.6251(2)
$z$ (S1)	0.3781(6)	0.3789(4)	0.3778(7)	0.3751(11)
$z$ (S2)	0.8119(4)	0.8118(3)	0.8143(6)	0.8160(9)
$U_{\text{iso}}$ (RE) ( $\text{\AA}^2$ )	0.0080(5)	0.0097(4)	0.0084(7)	0.0109(10)
$U_{11}$ (Bi) ( $\text{\AA}^2$ )	0.0096(4)	0.0093(3)	0.0102(6)	0.0148(9)
$U_{33}$ (Bi) ( $\text{\AA}^2$ )	0.0265(11)	0.0211(7)	0.0254(14)	0.022(2)
$U_{11}$ (S1) ( $\text{\AA}^2$ )	0.032(3)	0.021(2)	0.017(3)	0.008(4)
$U_{33}$ (S1) ( $\text{\AA}^2$ )	0.037(6)	0.027(4)	0.036(7)	0.060(10)
$U_{\text{iso}}$ (S2) ( $\text{\AA}^2$ )	0.007(2)	0.0071(12)	0.005(2)	0.011(4)